Brownian transport in corrugated channels with inertia

P. K. Ghosh, P. Hänggi, F. Marchesoni, F. Nori, and G. Schmid

Brownian transport in corrugated channels with inertia

P. K. Ghosh,[1, 2] P. Hänggi,[2] F. Marchesoni,[3] F. Nori,[1] and G. Schmid[2]

[1] *Advanced Science Institute, RIKEN, Wako-shi, Saitama, 351-0198, Japan*
[2] *Institut für Physik Universität Augsburg, D-86135 Augsburg, Germany*
[3] *Dipartimento di Fisica, Università di Camerino, I-62032 Camerino, Italy*

Transport of suspended Brownian particles dc driven along corrugated narrow channels is numerically investigated in the regime of finite damping. We show that inertial corrections cannot be neglected as long as the width of the channel bottlenecks is smaller than an appropriate particle diffusion length, which depends on the the channel corrugation and the drive intensity. With such a diffusion length being inversely proportional to the damping constant, transport through sufficiently narrow obstructions turns out to be always sensitive to the viscosity of the suspension fluid. The inertia corrections to the transport quantifiers, mobility and diffusivity, markedly differ for smoothly and sharply corrugated channels.

I.   INTRODUCTION

Brownian transport in narrow corrugated channels is a topic of potential applications to both natural [1–3] and artificial devices [4]. Depending on the amplitude and geometry of the wall modulation, corrugated channels fall within two distinct categories, see Fig. 1: (i) smoothly corrugated channels. Also called entropic channels [5], these quasi one dimensional (1D) channels were introduced first in Ref. [6] and further investigated in Refs. [7–14], as an instance of two (2D) or three dimensional (3D) systems describable in terms of an effective 1D kinetic equation. These are typically modeled as periodic channels with axial symmetry and unit cells delimited by bottlenecks which are assumed to be narrow with respect to the cell dimensions, i.e., the channel cross section and the period; (ii) compartmentalized (or septate) channels [15–21]. These channels are sharply corrugated channels formed by identical compartments separated by thin dividing walls and connected by narrow openings (pores) centered around their axis. At variance with the case of smoothly corrugated channels, diffusion in compartmentalized channels cannot be reduced to an effective 1D kinetic process directed along the axis. Accordingly, driven transport in such strongly constrained geometries exhibits distinct features, which cannot be reconciled with the known properties of Brownian motion in quasi-1D systems [3, 22, 23].

Corrugated channels are often used to model transport of dilute mixtures of small particles (like biomolecules, colloids or magnetic vortices) in confined geometries [4]. Each particle is subjected to thermal fluctuations with temperature T and large viscous damping constant γ, and a homogeneous constant force directed locally parallel to the channel axis. Such a dc drive is applied from the outside by coupling the particle to an external field (for instance, by attaching a dielectric or magnetic dipole, or a magnetic flux to the particle), without inducing drag effects on the suspension fluid. Interparticle and hydrodynamic interactions can thus be ignored; for a more
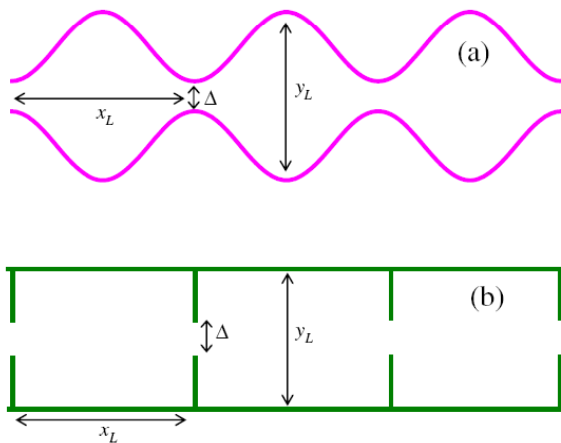

FIG. 1: (Color online) Sketch of a smoothly corrugated (a) and a compartmentalized 2D channel (b) directed along the x axis. In both cases the channel unit cell is x_L long and y_L wide; the radius of the connecting bottlenecks or pores is Δ.

detailed discussion on the validity of this simplifying assumption we refer the readers to Refs. [5, 14].

In this paper we investigate the relevance of the inertia effects due to the viscosity of the suspended particle. As is often the case with biological and most artificial suspensions [4], the Brownian particle dynamics in the bulk can be regarded as overdamped. This corresponds to (i) formally setting the mass of the particle to zero, $m = 0$, or, equivalently, to make the friction strength γ tend to infinity, and (ii) assuming F smaller than the thermal force $F_0 = \gamma\sqrt{kT/m}$; for the validity and the corrections to the Smoluchowski approximation see in cited Refs. [28]. The current literature on corrugated channels invariably assumes such an overdamped limit. But how large is an "infinite" γ (or how small a "zero" m)? The answer, of course, depends on the geometry of the channel.
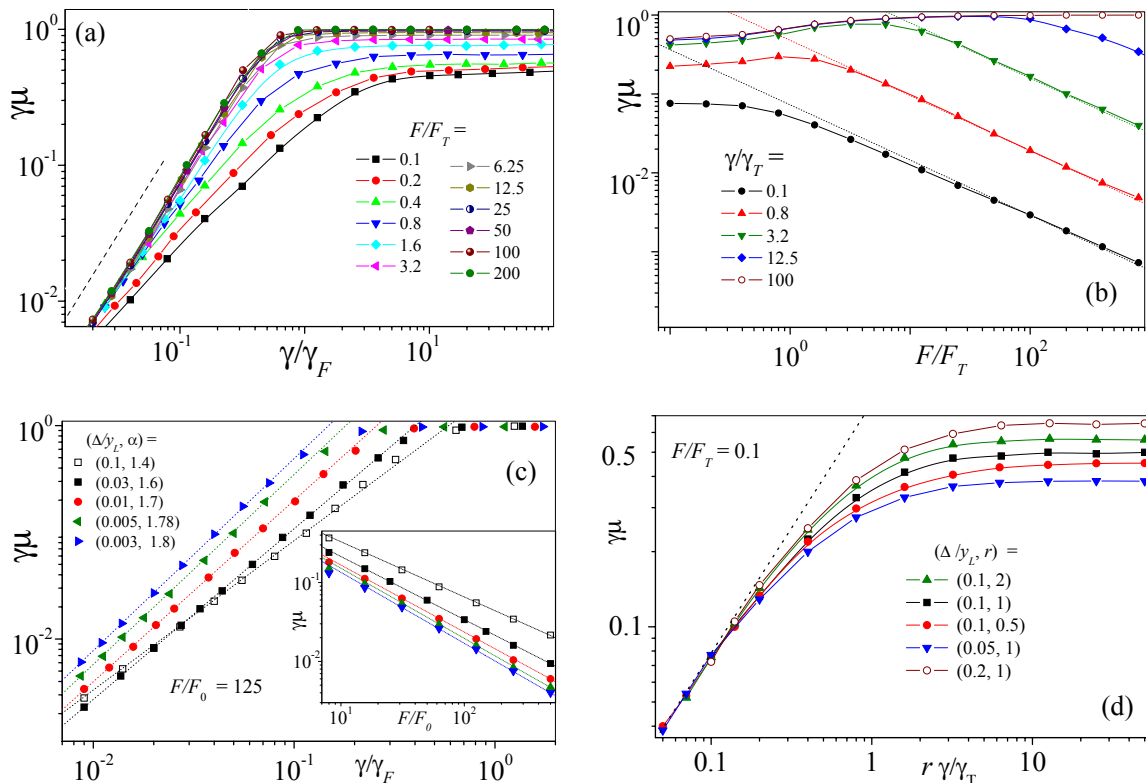
Our main conclusion is that the overdamped dynam-

FIG. 2: (Color online) Rescaled mobility, $\gamma\mu$, in a smoothly corrugated channel with $r = x_L/y_L = 1$, $\Delta/y_L = 0.1$, and (a) vs. γ/γ_F for different F; (b) vs. F/F_T for different γ. The relevant scaling parameters are $F_T = kT/\Delta$, $\gamma_T = \sqrt{mkT}/\Delta$, Eq. (8), and $\gamma_F = \sqrt{mF/\Delta}$, Eq. (9). The dashed lines represent, respectively, the fitting power laws $(\gamma/\gamma_F)^\alpha$ in (a) and $(F/F_T)^{-\alpha/2}$ in (b), both with $\alpha = 1.4$ (see Sec. III). In (c) $\gamma\mu$ is plotted vs. γ/γ_F (main panel) and F/F_0 (inset) for $\gamma/\gamma_T = 0.8$, $F/F_T = 125$, and different cross-section ratios, Δ/y_L. The corresponding fitting exponents α are also reported in the legend. In the inset, F is expressed in units of F_0 instead of F_T for graphical reasons. The dependence of $\gamma\mu$ on the geometry of the channel unit cell for low damping and small drives is illustrated in (d), where $\gamma\mu$ is plotted vs. $r\gamma/\gamma_T$. The predicted linear law with slope $\pi/4$ [32] is represented by a dotted line [see also Eq. (12) and text following].

ics assumption for Brownian diffusion through pores of width Δ subjected to a homogeneous drive F, applies only for $\gamma \gg \sqrt{mkT}/\Delta$, and $\gamma \gg \sqrt{mF/\Delta}$ [28], irrespective of the degree of corrugation. This means that inertial correction cannot be neglected as long as Brownian diffusion is spatially correlated on a length ($l_T = \sqrt{mkT}/\gamma$ at small dc drive, or $l_F = mF/\gamma^2$ at large dc drive) of the order of or larger than the pore width Δ. Therefore, for sufficiently narrow pores or sufficiently large drives, inertia always comes into play by enhancing the blocking action of the channel bottlenecks.

This paper is organized as follows. In Sec. II we introduce the Langevin equation formalism employed in our simulation code. Simulation data for the particle mobility and diffusivity are analyzed in Sec. III as functions of the drive, the channel geometry, and the damping constant in sinusoidally corrugated channels. We report significant deviations from the best known overdamped regime. In Sec. IV we consider the case of septate channels for which dependable fitting formulas could be analytically obtained. Inertial effects in these two limiting corrugation regimes are compared in Sec. V. Finally, in

Sec. VI we add some concluding remarks.

II. MODEL

Let us consider a point-like Brownian particle of mass m diffusing in a 2D suspension fluid contained in a periodic channel with unit cell $x_L \times y_L$, as illustrated in Fig. 1. The particle is subjected to a homogeneous force $\vec{F}$. The damped dynamics of the particle is modeled by the 2D Langevin equation,

$$m\frac{d^2\vec{r}}{dt^2} = -\gamma\frac{d\vec{r}}{dt} + \vec{F} + \sqrt{\gamma kT}\,\vec{\xi}(t), \qquad (1)$$

where $\vec{r} = (x, y)$. The random forces $\vec{\xi}(t) = (\xi_x(t), \xi_y(t))$ are zero-mean, white Gaussian noises with autocorrelation functions $\langle \xi_i(t)\xi_j(t')\rangle = 2\delta_{ij}\delta(t-t')$, with $i, j = x, y$. Here, γ plays the role of an effective viscous damping constant incorporating all additional effects that are not explicitly accounted for in Eq. (1), like hydrodynamic drag, particle-wall interactions, etc. We numerically integrated

Eq. (1) by a Milstein algorithm [29]. The stochastic averages reported in the forthcoming sections were obtained as ensemble averages over 10^6 trajectories with random initial conditions; transient effects were estimated and subtracted.

As anticipated in Sec. I, we considered two categories of periodic channels, smoothly corrugated and septate channels. The symmetric walls of smoothly corrugated channels have been modeled by the sinusoidal functions $\pm w(x)$, where

$$w(x) = \frac{1}{4}\left[(y_L + \Delta) - (y_L - \Delta)\cos\left(\frac{2\pi x}{x_L}\right)\right], \quad (2)$$

see Fig. 1(a)]. The compartments of the septate channels are rectangular and the dividing walls have zero width, see Fig. 1(b).

Two quantifiers have been used to best represent the different transport properties of these two channel geometries in the overdamped limit, $\gamma \to \infty$:

(i) mobility. The response of a Brownian particle in a channel subjected to a dc drive, F, oriented along the axis direction, x, is expressed by the mobility,

$$\mu(F) = \langle v(F)\rangle/F, \quad (3)$$

where $\langle v\rangle \equiv \langle \dot{x}(F)\rangle = \lim_{t\to\infty}[\langle x(t)\rangle - x(0)]/t$. In entropic channels $\mu(F)$ increases from a relatively small value for $F = 0$, μ_0, up to the free-particle limit, $\gamma\mu_\infty = 1$, for $F \to \infty$ [11]. We recall that in a smooth channel a free particle drifts with speed $v_\infty = F/\gamma$, that is, with $\gamma\mu = 1$. On the contrary, in compartmentalized channels $\gamma\mu(F)$ decreases monotonically with increasing F towards a geometry dependent asymptotic value, $\gamma\mu_\infty$, equal to the ratio of the pore to the channel cross-section [15], that is

$$\gamma\mu_\infty = \Delta/y_L, \quad (4)$$

(ii) diffusivity. As a Brownian particle is driven across a periodic array of bottlenecks or compartment pores, its diffusivity,

$$D(F) = \lim_{t\to\infty}[\langle x^2(t)\rangle - \langle x(t)\rangle^2]/2t, \quad (5)$$

picks up a distinct F dependence. In entropic channels with smooth bottlenecks, for $F \to \infty$ the function $D(F)$ approaches the free diffusion limit, $D(\infty) = D_0$, after going through an excess diffusion peak centered around an intermediate (temperature dependent [11]) value of the drive. The bulk or free diffusivity, D_0, is proportional to the temperature, $D_0 = kT/m\gamma$. Such a peak signals the depinning of the particle from the entropic barrier array [30]. In compartmentalized channels, instead, $D(F)$ exhibits a distinct quadratic dependence on F [17, 19], reminiscent of Taylor's diffusion in hydrodynamics [31], that is, for $\Delta \ll y_L$,

$$\frac{D(F)}{D_0} = \frac{1}{2}\left(\frac{F\Delta}{kT}\right)^2. \quad (6)$$

This observation suggests that the particle never frees itself from the geometric constriction of the compartment pores, no matter how strong F.

These two quantifiers of mobility and diffusivity can also be used to assess the magnitude of the inertia effects. We remind here that, in the absence of external drives and for any value of the damping constant, Sutherland-Einstein relation [24–27]:

$$\gamma\mu_0 = D(0)/D_0, \quad (7)$$

establishes the dependence of the transport parameters on the temperature and the channel compartment geometry under equilibrium conditions [15].

In preparation for the quantitative analysis of our numerical data, we remark that Eq. (1) can be conveniently rewritten in terms of the rescaled units $t \to \gamma t/m$ and x/l_T, with $l_T = \sqrt{mkT}/\gamma$. A straightforward dimensional argument shows that, for any given channel unit cell $x_L \times y_L$, both the particle rescaled mobility, $\gamma\mu$, Eq. (3), and its rescaled diffusivity, D/D_0, Eq. (5), are functions of the rescaled drive, F/F_0, with $F_0 = \gamma\sqrt{kT/m}$, and three cell parameters, typically, the pore width, Δ/l_T, the pore-to-channel cross-section ratio, Δ/y_L, and the compartment aspect-ratio, $r = x_L/y_L$ (see Table I). Note that a simultaneous rescaling of all lengths by a factor κ would correspond to a noise intensity rescaling, $T \to T/\kappa^2$. Throughout our simulations we assumed narrow channels with small bottlenecks, meaning that $x_L \geq y_L$ and $\Delta \ll y_L$.

III. CORRUGATED CHANNELS

As anticipated in a preliminary report [32], inertial effects in corrugated channels become apparent both for small γ and for large F. Upon inspecting Fig. 2 we realize that inertia tends to suppress the particle mobility through the channel bottlenecks. Indeed, in the underdamped limit, $\gamma \to 0$, the rescaled mobility drops to zero, no matter what F [Fig. 2(a)]. In particular, when expressing γ in units of $\gamma_F = \sqrt{mF/\Delta}$, see Eq. (9) below, the mobility curves at large drives tend to collapse on a universal curve well fitted by the power law $(\gamma/\gamma_F)^\alpha$ with $\alpha = 1.4$. Correspondingly, in Fig. 2(b) the mobility decays like $F^{-\alpha/2}$ for small $F \gg F_T$.

The power law, $\gamma\mu \propto (\gamma/\gamma_F)^\alpha$, introduced here is only a convenient fit of the rescaled mobility function, even if it holds for two or more decades of γ/γ_F. [Note that the power law $\gamma\mu \propto F^{-\alpha/2}$ works throughout the entire F range explored in Fig. 2(b).] The analytical form of that function remains to be determined. The data reported in Fig. 2(c) clearly suggests that the fitting exponent, α, slightly depends on Δ, with $\alpha \to 2$ in the limit $\Delta \to 0$.

The dependence of the rescaled mobility on the system parameters in the underdamped limit is further illustrated in Fig. 2(d), where at low γ and for vanishingly small drives, the mobility grows proportional to the as-

TABLE I: Summary of characteristic scaling parameters and their meaning

$F_0 = \gamma\sqrt{\frac{kT}{m}}$	Thermal force: viscous force experienced by a Brownian particle with thermal velocity $v_{th} = \sqrt{kT/m}$.
$D_0 = \frac{kT}{\gamma}$, $v_\infty = \frac{F}{\gamma}$	Free diffusivity and velocity in bulk.
$l_T = \frac{\sqrt{mkT}}{\gamma}$	Thermal length: distance covered by a Brownian particle diffusing with thermal velocity v_{th} in the relaxation time, m/γ.
$l_F = \frac{mF}{\gamma^2}$	Ballistic length: distance covered by a driven Brownian particle drifting with velocity v_∞ in the relaxation time, m/γ.
$\gamma_T = \frac{\sqrt{mkT}}{\Delta}$	Damping cut-off at the pore (zero drive): $l_T = \Delta$.
$\gamma_F = \sqrt{\frac{mF}{\Delta}}$	Damping cut-off at the pore (strong drive): $l_F = \Delta$.
$D_T = \frac{kT}{\gamma_T}$, $F_T = \frac{kT}{\Delta}$	Scaling parameters introduced in Figs. 2-5; obtained by replacing γ with γ_T, respectively, in D_0 and F_0.

pect ratio $r = x_L/y_L$ of the channel unit cell and the pore cross section Δ.

Deviations from the expected overdamped behavior are the more prominent in the diffusivity data. As shown in Fig. 3, at large γ the curves $D(F)$ approach the horizontal asymptote $D(F) = D_0$, as expected [11]. However, beyond a certain value of F, seemingly proportional to γ^2 (inset), these curves abruptly part from their horizontal asymptote with a sort of cusp. In the underdamped limit, the F dependence of the diffusivity bears no resemblance with the typical overdamped behavior. At low γ, all $D(F)$ data sets collapse on a unique curve [Fig. 3, inset], which tends to a value smaller than D_0 for $F \to 0$, and diverges for $F \to \infty$, like F^β with $\beta \simeq 1$. Such power law holds for large γ, as well, though for sufficiently large F, only. Indeed, for exceedingly large F, all $D(F)$ curves seem to eventually approach a unique asymptote, irrespective of γ.

By comparing the plots of Figs. 2-3 we conjecture that corrections due to inertia become significant in two regimes, namely:
(i) at *low drives*, under the condition

$$\gamma \lesssim \gamma_T = \sqrt{mkT}/\Delta . \qquad (8)$$

This characteristic damping was used to rescale the mobility data in Fig. 1 [see also Fig. 2(b), inset]; moreover, in Fig. 3, for $\gamma < \gamma_T$ the diffusivity becomes a monotonic function of F with no plateau around D_0. The physical meaning of γ_T is simple. For $\gamma < \gamma_T$ the *thermal* length $l_T = \sqrt{mkT}/\gamma$ grows larger than the width of the pores, Δ, so that the Brownian particle cannot reach the nor-

mal diffusion regime, implicit in the Sutherland-Einstein relation, before bouncing off the pore walls. As a consequence, the Smoluchowski approximation fails in the vicinity of the bottlenecks.

Replacing γ with γ_T in the bulk quantities D_0 and F_0 yields, respectively, $D_T = kT/\gamma_T$ and $F_T = kT/\Delta$. These are the γ-independent rescaling factors introduced in Figs. 2-3 to characterize the inertia effects of the pore constrictions;
(ii) at *high drives* for

$$\gamma \lesssim \gamma_F = \sqrt{mF/\Delta} . \qquad (9)$$

As pointed out in Ref. [19], the large drive regime sets on when the length scale of the longitudinal particle distribution grows smaller than the pore size, namely for $F \gg F_T$. In the presence a strong dc drive, the condition $\gamma \gg \gamma_T$ does not suffices to ensure normal diffusion: the additional condition that $\Delta \gg l_F$ is required. Here, $l_F = mF/\gamma^2$ represents the *ballistic* length of a driven-damped particle, that is an estimate of the bouncing amplitude of a driven particle against the bottleneck. Upon increasing F at constant γ, l_F eventually grows larger than Δ and inertia comes into play. This mechanism is clearly responsible for the abrupt increasing branches of $D(F)$ in Fig. 3. A synoptic comparison of all characteristic scaling parameters of the system is displayed in Table I.

In conclusion, low and large drive limits are quantitatively defined as $F \ll F_T$ and $F \gg F_T$, respectively. As γ_F was introduced to characterize the large drive (ballistic) regime, clearly $\gamma_F > \gamma_T$. This means that applying
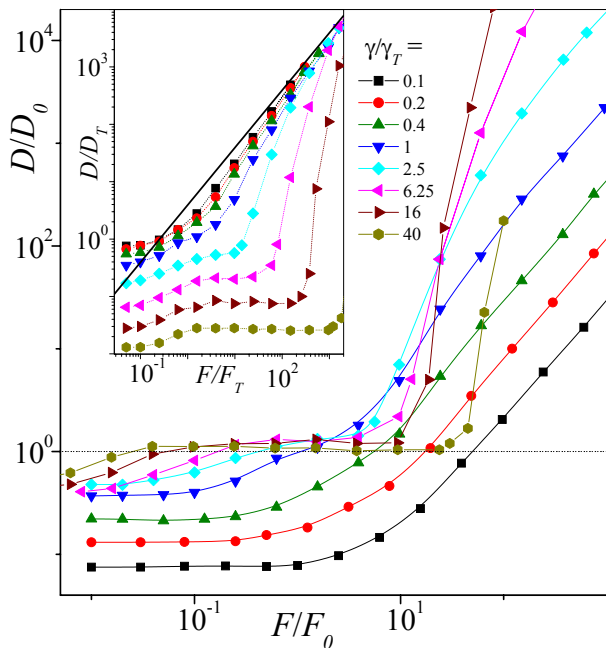
FIG. 3: (Color online) Rescaled diffusivity, D/D_0, vs. F/F_T (main panel) and D/D_T vs. F/F_0 (inset) in the corrugated channel of Eq. (2) with $r = 1$, $\Delta/y_L = 0.1$, and different γ. The scaling parameters introduced here are $D_T = kT/\gamma_T$ and $F_0 = \gamma\sqrt{kT/m}$. The solid line in the inset is the heuristic power law of Eq. (17).

a large external drive makes the effects of inertia all the stronger. On the other hand, if we decrease Δ, while keeping F constant, inertia effects are controlled by γ_T rather than by γ_F, as eventually $\gamma_T > \gamma_F$. The smooth crossover between these two regimes is responsible for the weak Δ dependence of the fitting exponent α in Fig. 2.

An analytical derivation of the transport quantifiers in the presence of strong inertial effects (low γ and/or large F) proved a difficult task. This is the case, for instance, of the universal mobility curve in the inset of Fig. 2(a). To gain a deeper insight on this and related issues we address next the particular case of a rectangular compartmentalized channel.

IV. SEPTATE CHANNELS

The role of inertia in compartmentalized channels is illustrated by the plots of Fig. 4. In panel (a) the rescaled mobility curve $\gamma\mu(F)$ at low damping exhibits a horizontal asymptote for $F \to \infty$. However, in comparison with the overdamped case reported in Sec. II, such an asymptote is proportional to Δ only for relatively narrow pores (see also inset) and is strongly suppressed with decreasing γ. The dependence of the mobility on the damping constant is better illustrated in panel (b), where $\gamma\mu$ linearly increases with γ before reaching the limit predicted in the overdamped regime [15, 17–19]. Similar behaviors
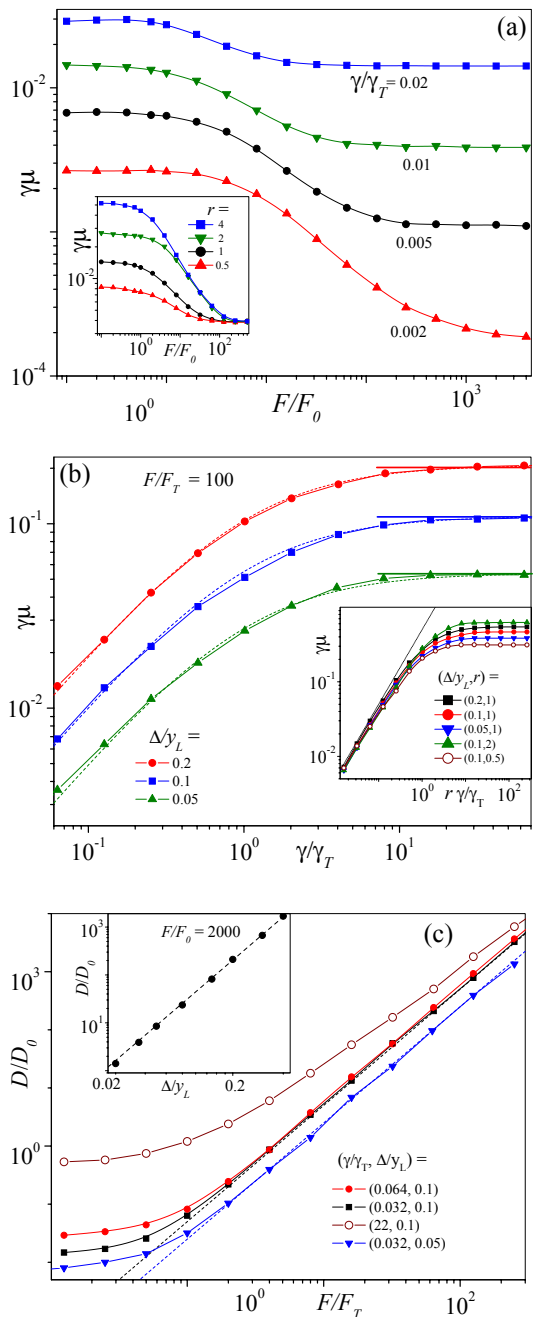

FIG. 4: (Color online) Transport in a compartmentalized channel with $r = x_L/y_L = 1$: rescaled mobility, $\gamma\mu$, vs. F/F_0 (a) and vs. γ/γ_T (b); diffusivity, D/D_0, vs. F/F_T (c). The remaining simulation parameters are reported in the legends. The relevant scaling parameters are $F_0 = \gamma\sqrt{kT/m}$, $F_T = kT/\Delta$, and $\gamma_T = \sqrt{mkT}/\Delta$. Inset of (a): $\gamma\mu$ vs. F/F_T for different r and Δ/y_L. Inset of (b): $\gamma\mu$ vs. γ/γ_T for different Δ/y_L and r. Inset of (c): D/D_0 vs. Δ/y_L for $F/F_T = 2\,10^3$. The dotted curves represent the approximate analytical expressions of Eqs. (11) and (15), respectively for the mobility in (b) and the diffusivity in (c) (main panel and insets). In (b) the quantity $\gamma\mu|_\infty$ was estimated from the horizontal asymptotes. Note that $\gamma\mu_\infty$ (see Sec. II) is known to be proportional to Δ for $F \to \infty$ [horizontal arrows, Eq. (4)], and to $|\ln \Delta|$ for $F \to 0$ [19].

were observed both at low (inset) and large drives (main panel). For large drives the rescaled mobility actually converges toward the estimate $\gamma\mu|_\infty$ of Eq. (4).

The dependence of the rescaled mobility on the compartment geometry is further illustrated in the inset of Fig. 4(b): in the zero drive limit and for low γ, the mobility is proportional to the aspect ratio $r = x_L/y_L$ and the pore size, Δ, as already reported for the corrugated channels of Fig.2(d).

Contrary to the smoothly corrugated channels of Sec. III, the drive dependence of the diffusivity is apparently not much affected by inertia. As shown in Fig. 4(c), the curves $D(F)$ keep diverging quadratically with F, irrespective of the compartment size and the damping constant, like in the overdamped limit. In the notation introduced above for the corrugated channel, $D(F)$ scales like F^β but, contrary to Fig. 3, here $\beta = 2$. The power law dependence of $D(F)$ on the pore size and the channel width is displayed in the insets of Fig. 4(c).

Although of lesser applicability, septate channels have a practical advantage over smoothly corrugated channels, as they are characterized by well distinct time scales, which often allow convenient analytical approximations. The problem under study is no exception.

Let us consider first the rescaled mobility at large drives, $F \gg F_T$. As anticipated in Secs. I and III, two time scales control the particle current through the channel: (i) the bulk relaxation time, m/γ, and (ii) the ballistic time across the pore, m/γ_T. The latter is a measure of transient effects that may be detected only at the shortest distances, here, the pore width. To bridge the above time scales we introduce the effective relaxation time $\tau_{\text{eff}} = m/\gamma_{\text{eff}}$, where the effective damping constant is defined as

$$\gamma_{\text{eff}} = \gamma(1 + \gamma_T/\gamma). \tag{10}$$

Correspondingly, the rescaled mobility function can be approximated to

$$\gamma\mu = \frac{\gamma\mu|_\infty}{1 + \gamma_T/\gamma}, \tag{11}$$

where $\gamma\mu|_\infty$ denotes the rescaled mobility in the overdamped limit, $\gamma \to \infty$. Despite its being a simple interpolating formula, Eq. (11) fits quite closely the simulation curves of Figs. 4(a) and (b) for large drives (main panel). Note that the horizontal asymptotes for large γ coincide with the expected values of $\gamma\mu|_\infty$, whose dependence on the compartment geometry, noise and drive intensity is analytically known [17–20].

Let us consider next the rescaled mobility at low drives, $F \ll F_T$. For $F = 0$ the transport quantifiers $\gamma\mu_0$ and $D(0)$ can be formally expressed in terms of the mean exit time, $\bar\tau_e$, of the Brownian particle out of a single compartment, namely, $D(0) = x_L^2/4\bar\tau_e$ and $\mu_0 = D(0)/kT$, see Eq. (7). An analytical expression for $\bar\tau_e$ as a function of the compartment geometry is only available in the overdamped dynamics approximation [33]. In the absence of

a fully analytical treatment, we interpret the numerical results shown in the inset of Fig. 4(b) by assuming a 1D collisional dynamics along the x axis. At very low damping and $F = 0$, the particle bounces off the same compartment wall with rate $2v_{\text{th}}/x_L$ (attack frequency), but only a fraction Δ/y_L of such collisions leads to a pore crossing. As a consequence, $\bar\tau_e \sim x_L y_L/2\Delta\sqrt{kT/m}$ and

$$\gamma\mu_0 \sim \frac{\gamma x_L}{2\sqrt{mkT}}\frac{\Delta}{y_L} = \frac{r}{2}\frac{\gamma}{\gamma_T}, \tag{12}$$

which reproduces with the linear fit in the inset of Fig. 4(b). Note that such a qualitative argument applies to the weakly corrugated channels of Fig. 2(c), as well. In that case, however, v_{th} must be replaced by $(2/\pi)v_{\text{th}}$, to account for an almost isotropic 2D distribution of the ballistic trajectories inside the compartment; correspondingly, the factor $1/2$ on the r.h.s. of Eq. (12) should be changed to $\pi/4$, see Fig. 2(d).

The scaling law of the diffusivity at large drives, $D(F) \propto F^\beta$ with $\beta = 2$, can be quantitatively determined by generalizing an argument originally introduced for the overdamped regime [19]. For large F, the instantaneous particle velocity, $v(t) \equiv \dot{x}(t)$, switches between a locked mode with $v_0 = 0$, as it sticks against a compartment wall, and a running mode with $v_\infty = F/\gamma$, as it runs along the central lane of the channel. In view of Eq. (4), it is clear that the particle spends a fraction $1-\Delta/y_L$ of the time in the locked mode, and the remaining Δ/y_L of the time in the running mode. The random variable $v(t)$ can thus be modeled as a dichotomic process with subtracted autocorrelation function [34]

$$
\begin{aligned}
C(t) &\equiv \lim_{s\to\infty}[\langle v(t+s)\rangle - \langle v\rangle][\langle v(s)\rangle - \langle v\rangle] \\
&= (v_\infty - v_0)^2\frac{\bar\tau_0\bar\tau_\infty}{\bar\tau^2}\,\exp\left(-\frac{\bar\tau t}{\bar\tau_0\bar\tau_\infty}\right),
\end{aligned}
$$

where $\bar\tau_0 = (1 - \Delta/y_L)\bar\tau$ and $\bar\tau_\infty = (\Delta/y_L)\bar\tau$ are the average permanence times, respectively, in the locked and running mode; their sum, $\bar\tau$, is the relaxation time constant of the dichotomic process, still to be determined. The spatial diffusivity $D(F)$ can be obtained by integrating $C(t)$ over time and then making use of the explicit expressions for v_0, v_∞, $\bar\tau_0$, and $\bar\tau_\infty$, namely

$$D(F) = \int_0^\infty C(t)dt = \left(\frac{F}{\gamma}\right)^2\left[\frac{\Delta}{y_L}\left(1 - \frac{\Delta}{y_L}\right)\right]^2\bar\tau. \tag{13}$$

To determine the unknown time constant $\bar\tau = (y_L/\Delta)\bar\tau_\infty$, we notice that a particle remains in the running mode for a time $\bar\tau_\infty$ of the order of the time it takes to diffuse out of the central channel lane, namely, for low damping,

$$2D_0\tau_\infty = \frac{1}{4}[(y_L + \Delta)^2 - (y_L - \Delta)^2]. \tag{14}$$

By inserting the analytical expression for τ_∞ thus derived into Eq. (13) and taking for simplicity the limit of narrow pores, $\Delta \ll y_L$, one arrives at

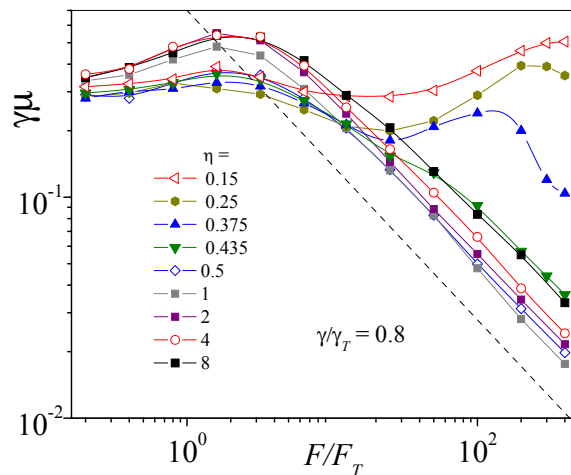$$\frac{D(F)}{D_0} = \frac{\Delta}{2y_L}\left(\frac{F}{F_T}\right)^2. \tag{15}$$

FIG. 5: (Color online) Channel with tunable corrugation, Eq. (16): rescaled mobility, $\gamma\mu$ vs. F/F_T for different *eta*. Other simulation parameters: $r = 1$, $\Delta/y_L = 0.1$, and $\gamma/\gamma_T = 0.8$. The dashed line is the power law $(F/F_T)^{-\alpha/2}$ with $\alpha = 1.4$ drawn in Fig. 2(b) for $\eta = 2$.

This expression is independent of γ and well reproduces all simulation data of Fig. 4(b) at large F or, more precisely, under the condition that $\gamma \ll \gamma_F$.

On comparing the asymptotic laws for the diffusivity at $\gamma \to 0$, Eq. (15), and at $\gamma \to \infty$, Eq.(6), one would expect $D(\gamma \to 0)/D(\gamma \to \infty) = \Delta/y_L$. On the contrary, in Fig. 4(c) we immediately notice that all $D(F)$ curves approach the same asymptotic scaling law, Eq.(6). As discussed for the corrugated channels, the overdamped diffusion scaling law, Eq. (15), holds only under the condition that $\gamma \gg \gamma_F$. Correspondingly, here as well, increasing F such that $F > \gamma^2\Delta/m$, or $l_F \gg \Delta$, makes inertia effects on confined diffusion emerge (though in a less dramatic way).

V. DISCUSSION

The comparison between transport properties in smoothly and sharply corrugated channels is suggestive of the role played by the channels profile in the presence of inertia. In principle, both channel geometries of Sec. III and IV could be reproduced by means of one parametric profile function, say,

$$w_\eta(x) = \frac{1}{2}\left[\Delta + (y_L - \Delta)\sin^\eta\left(\frac{\pi x}{x_L}\right)\right], \quad (16)$$

with tunable exponent η [35]. This function coincides with $w(x)$, Eq. (2), for $\eta = 2$ and approaches a rectangular compartment $x_L \times y_L$ for $\eta \to 0$. The divide between smoothly and sharply corrugated channels can be set at $\eta = 1$, where the two sides of the bottleneck profile change from concave, for $\eta > 1$, to convex, for $\eta < 1$. Such change in the pore geometry affects, for instance, the drive dependence of the rescaled mobility at

low damping, see Fig. 5. All curves $\gamma\mu(F)$ with $\eta > 1$ decay with the same approximate power law as reported in Fig. 2(b) for $\eta = 2$. For $\eta < 1$, instead, the behavior of $\gamma\mu(F)$ is as in Fig. 2(b) (sinusoidally corrugated channel), at low F, and in Fig. 4(a) (septate channel), at large F. Without further analyzing the η dependence of the transport quantifiers, we now discuss certain differences and similarities between sinusoidal and septate channels.

In both types of channels, the diffusivity grows asymptotically with the drive according to a power law, $D(F) \propto F^\beta$, where $\beta = 2$ for septate channels and $\beta = 1$ for sinusoidal channels. For smoothly corrugated channels this result may come as a surprise, since, for large damping, the diffusivity is known to approach its bulk value, $D(F \to \infty) = D(0)$. The asymptotic power law with $\beta = 1$ illustrated in the inset of Fig. 3 results from the enhanced trapping effect due to the underdamped particle bouncing back and forth against the compartment walls. A simple qualitative argument yields [32]

$$\frac{D(F)}{D_T} \sim \frac{\pi}{8}\frac{x_L F}{kT} = r\frac{\pi}{8}\frac{y_L}{\Delta}\frac{F}{F_T}, \quad (17)$$

in rather good agreement with our simulation data (see inset of Fig. 3). Note that, lowering the temperature, for small damping $D(F)$ diverges like $T^{-1/2}$, which means that diffusion is the result of chaotic ballistic collisions.

Inertia corrections to the drive dependence of the diffusivity are not as dramatic in septate channels, Fig. 4(c), as they appear in corrugated channels, Fig. 3. This explains why the role of the threshold γ_F, Eq. (9), is less prominent for sharply corrugated channels. On a closer look, however, one notices that, on increasing γ, the data points for $D(F)/D_0$ approach the predicted oblique asymptote of Eq. (15) at larger and larger F, consistently with the large-drive inertial regime $\gamma \ll \gamma_F$.

Finally, we notice that septate and sinusoidally corrugated channels also differ in the large-drive behavior of their mobilities at low damping. While in septate channels $\gamma\mu(F \to \infty)$ was shown to approach a small but finite value, $\gamma\mu|_\infty(\gamma/\gamma_T)$, see Eq. (11), the mobility in sinusoidal channels was numerically fitted by the scaling law $\gamma\mu(F \to \infty) \sim (\gamma/\gamma_F)^\alpha$, where α is an increasing function of Δ with $\alpha(\Delta \to 0) = 2$ [Fig. 2(c)]. This means that in sinusoidal channels $\langle v(F)\rangle$ [and not $\gamma\mu(F)$] tends to a finite asymptotic value. By definition, the rescaled mobility can be written as $\gamma\mu \sim (x_L/\bar{\tau}_d)(\gamma/F)$, where $\bar{\tau}_d$ denotes the mean drift time of a particle across a compartment in the presence of a strong drive. Accordingly, as $\alpha \to 2$, the drift time $\bar{\tau}_d$ becomes insensitive to the (large) drive, which hints at an emerging ballistic dynamics [36]. We also remark that the above scaling law for $\gamma\mu(F \to \infty)$ applies to all pore geometries with $\eta \geq 1$ [35], see Fig. 5; for septate channels, $\eta \to 0$, such a scaling law, with $1 < \alpha < 2$, closely reproduces the decaying branch of the mobility curves displayed in Fig. 4(a).

VI. CONCLUSIONS

The main result of this work is that for real physical suspensions flowing through confined geometries, both in biological and artificial systems, pore crossings grow increasingly sensitive to the suspension fluid viscosity with decreasing the pore radius. With respect to previous attempts at incorporating finite-mass effects in the analysis of Brownian transport through corrugated narrow channels [37–39], we stress that the inertial effects reported here are not of mere academic interest [32].

Inertial effects can be directly observed, for instance, in a dilute solution of colloidal particles driven across a porous membrane or an artificial sieve [40, 41]. On the other hand, channel profiles at the micro- and nanoscales can be tailored as most convenient [42]. As detailed in Ref. [32], the experimental demonstration of inertial effects on Brownian transport through narrow pores is to become accessible when manipulating artificial particles of micrometric size by means of well established exper-

imental techniques [43–46]. For nano-particles, like biological molecules, detecting such effects will require more refined experimental setups.

[1] B. Hille, *Ion Channels of Excitable Membranes* (Sinauer, Sunderland, 2001).
[2] J. Kärger and D. M. Ruthven, *Diffusion in Zeolites and Other Microporous Solids* (Wiley, New York, 1992).
[3] H. Brenner and D. A. Edwards, *Macrotransport processes* (Butterworth-Heinemann, New York, 1993).
[4] P. Hänggi and F. Marchesoni, Rev. Mod. Phys. **81**, 387 (2009).
[5] for a review see: P.S. Burada, P. Hänggi, F. Marchesoni, G. Schmid, and P. Talkner, ChemPhysChem **10**, 45 (2009).
[6] R. Zwanzig, J. Phys. Chem. **96**, 3926 (1992).
[7] D. Reguera and J. M. Rubí, Phys. Rev. E **64**, 061106 (2001).
[8] P. Kalinay and J. K. Percus, Phys. Rev. E **74**, 041203 (2006).
[9] N. Laachi, M. Kenward, E. Yariv, and K. D. Dorfman, EPL **80**, 50009 (2007).
[10] D. Reguera, G. Schmid, P.S. Burada, J. M. Rubí, P. Reimann, and P. Hänggi, Phys. Rev. Lett. **96**, 130603 (2006).
[11] P. S. Burada, G. Schmid, D. Reguera, J. M. Rubi, and P. Hänggi, Phys. Rev. E **75**, 051111 (2007).
[12] R. Reichelt, S. Günther, J. Wintterlin, W. Moritz, L. Aballe, and T. O. Mentes, J. Phys. Chem. **127**, 134706 (2007).
[13] D. Mondal and D. S. Ray, Phys. Rev. E **82**, 032103 (2010); D. Mondal, M. Das, and D. S. Ray, J. Chem. Phys. **132**, 224102 (2010).
[14] D. Reguera, A. Luque, P. S. Burada, G. Schmid, J. M. Rubi, and P. Hänggi Phys. Rev. Lett. **108**, 020604 (2012).
[15] F. Marchesoni and S. Savel'ev, Phys. Rev. E **80**, 011120 (2009).
[16] F. Marchesoni, J. Chem. Phys. **132**, 166101 (2010).
[17] Yu. A. Makhnovskii, A. M. Berezhkovskii, and V. Yu. Zitserman, J. Chem. Phys. **131**, 104705 (2009).
[18] A. M. Berezhkovskii, L. Dagdug, Yu. A. Makhnovskii,

and V. Yu. Zitserman, J. Chem. Phys. **132**, 221104 (2010).
[19] M. Borromeo and F. Marchesoni, Chem. Phys. **375**, 536 (2010).
[20] M. Borromeo, F. Marchesoni, and P. K. Ghosh, Chem. Phys. **134**, 051101 (2011).
[21] P. Hänggi, F. Marchesoni, S. Savel'ev, and G. Schmid, Phys. Rev. E **82**, 041121 (2010).
[22] M. H. Jacobs, *Diffusion Processes* (Springer, New York, 1967).
[23] H. Risken, *The Fokker-Planck Equation*, 2nd ed. (Springer, Berlin, 1989).
[24] W. Sutherland, Phil. Mag. **9**, 781 (1905); see relation (3) therein.
[25] A. Einstein, Ann. Phys. **17**, 549 (1905); see the non-numbered relation below his numbered equation (2) therein.
[26] P. Hänggi and H. Thomas, Phys. Rep. **88**, 207 (1982).
[27] P. Hänggi and F. Marchesoni, Chaos **15**, 026101 (2005).
[28] V. I. Tikhonov, Avtomatika i Telemekhania **21**, 301 (1960); G. Wilemski, J. Stat. Phys. **14**, 153 (1976); U. M. Titulaer, Physica A **91**, 321 (1978); J. L. Skinner and P. Wolynes, Physica A **96**, 561 (1979); P. Hänggi, P. Talkner, and M. Borkovec, Rev. Mod. Phys. **62**, 251 (1990); see Eq. (4.10) therein.
[29] P. Kloeden and E. Platen, *Numerical Solutions of Stochastic Differential Equations* (Springer, Berlin, 1999).
[30] G. Costantini and F. Marchesoni, Europhys. Lett. **48**, 491 (1999).
[31] G.I. Taylor, Proc. R. Soc. (London) A **219**, 186 (1953).
[32] P. K. Ghosh, P. Hänggi, F. Marchesoni, P. Nori, and G. Schmid, EPL **98**, 50002 (2012).
[33] D. Holcman, N. Hoze, and Z. Schuss, Phys. Rev. E **84**, 021906 (2011) and references therein.
[34] C.W. Gardiner, *Handbook of Stochastic Methods* (Springer, Berlin, 2004).

[35] P. K. Ghosh and F. Marchesoni, J. Chem. Phys. **136**, 116101 (2012).

[36] P. Gaspard, *Chaos, Scattering and Statistical Mechanics* (Cambridge University Press, Cambridge, 1998).

[37] A. M. Berezhkovskii and A. Szabo, J. Chem. Phys. **135**, 074108 (2011).

[38] S. Martens, I. M. Sokolov, and L. Schimansky-Geier, J. Chem. Phys., **136**, 111102 (2012).

[39] P. Kalinay and J. Percus, arXiv:1204.1145.v1 (2012).

[40] J. E. Mark, *Polymer Data Handbook* (Oxford, New York, 1999).

[41] N. Garbow *et al.*, J. Phys.: Condens. Matter, **16**, 3835 (2004).

[42] C. Dekker, Nat. Nanotech. **2**, 209 (2007).

[43] T. Li, S. Kheifets, D. Medellin, and M. Raizen, Science **328**, 1673 (2010).

[44] R. Huang, I. Chavez, K. Taute, B. Lukic, S. Jeney, M. Raizen, and E. Florin, Nature Physics **7**, 576 (2011).

[45] T. Franosch, M. Grimm, M. Belushkin, F. Mor, G. Foffi, L. Forró, and S. Jeney, Nature **478**, 85 (2011).

[46] A. Jannasch, M. Mahamdeh, and E. Schäffer, Phys. Rev. Lett. **107**, 228301 (2011).